Impacts of device processing on contact interfaces to (010) β -Ga₂O₃

Kathleen T. Smith^a, Cameron A. Gorsak^b, Avijit Kalra^c, Bennett J. Cromer^b, Debdeep Jena^{b,d,e}, Hari P. Nair^b, and Huili G. Xing^{b,d,e}

^aSchool of Applied and Engineering Physics, Cornell University, Ithaca, NY 14853, USA
^bDepartment of Materials Science and Engineering, Cornell University, Ithaca, NY 14853, USA
^cSchool of Chemical and Biomolecular Engineering, Cornell University, Ithaca, NY 14853, USA
^dSchool of Electrical and Computer Engineering, Cornell University, Ithaca, NY 14853, USA
^eKavli Institute at Cornell for Nanoscale Science, Cornell University, Ithaca, NY 14853, USA

ABSTRACT

Metal-semiconductor interfaces to Ga_2O_3 have been demonstrated to be highly sensitive to device processing conditions. Liftoff processing leads to inconsistency in ohmic contact formation and quality due to apparent chemical modification of the surface layer, which is not affected by most traditional surface cleanings but can be removed by Ga-flux polishing. Metal-first processing on as-grown material, which avoids exposure of the Ga_2O_3 surface to photoresist prior to metal deposition, has been shown to form reliable, low-resistance ohmic contacts. Investigation of the chemical composition of contacts to material that has been modified by liftoff and cleaned by Ga-flux polishing by x-ray photoelectron spectroscopy (XPS) reveals slight variations in the oxidation states of the Ti and Ga in the contacts that indicate the nature of the surface chemistry modification.

Keywords: Gallium oxide, ohmic contacts, interfaces, liftoff

1. INTRODUCTION

Gallium oxide is an ultrawide bandgap semiconductor with favorable material properties that make it a promising candidate for power and RF electronics. Low-cost native substrates are readily available, and a wide range of in- and ex-situ doping densitities have been demonstrated across various epitaxial growth methods with electron mobilities up to nearly 200 cm²/V-s.^{1,2} The stable, monoclinic β -phase has a reported bandgap of 4.5-4.9 eV, and resultingly high critical electric field (E_c), which has already allowed for the demonstration of kilovolt MOSFET devices surpassing the unipolar limits of SiC and GaN.^{3,4} The high E_c allows for aggressive device scaling to minimize on-state conduction losses and results in lower leakage currents, especially at high temperatures; however, further improvements in device processing, particularly in control of the interfaces at metal ohmic and Schottky contacts, are needed to fully leverage this advantage.

Schottky contacts to Ga_2O_3 have been shown to suffer from Fermi-level pinning, meaning the measured barrier height does not increase linearly with the contact metal work function as predicted by the Schottky-Mott rule.⁵ Fermi-level pinning has been attributed to numerous factors including crystal orientation, trap states due to varying chemical composition caused by dopants or chemical treatments, and native defects such as vacancies and interstitials that may be promoted by different growth methods.^{6–10} While still not well-understood, the metal-semiconductor interface to Ga_2O_3 is clearly highly sensitive to the sample surface treatment and processing. Higher Schottky barriers are critical to reducing leakage current and observing the high E_c at device breakdown;¹¹ therefore, control of the interface quality both during material growth and device processing is critical.

Ohmic contacts, as well, have provided unexpected challenges. Despite demonstration of high quality, heavily doped contact regions via both in-situ doped epitaxial regrowth and ex-situ ion implantation with carrier concentrations $> 5 \times 10^{19}$ cm⁻³ (which is well above the Mott criteria) and carrier mobilities ~ 70 cm²/V-s, ¹ reported contacts are almost exclusively alloyed. While non-alloyed contacts are reported to form readily to $> 1 \times 10^{19}$ cm⁻³ doped GaN, contacts formed by liftoff processing to $> 5 \times 10^{19}$ cm⁻³ n+ doped epitaxial Ga₂O₃ has been shown to yield inconsistent results. ¹² Even reported non-alloyed contacts to $1-3 \times 10^{20}$ cm⁻³ doped Ga₂O₃ still improved by an order of magnitude after alloying. ¹³

Further author information: (Send correspondence to Kathleen T. Smith)

E-mail: kts57@cornell.edu

Here, we summarize previous discussions of the impact of device processing on the performance of ohmic contacts, particulary the observation that standard liftoff processing appears to chemically modify the oxide surface in a manner that inhibits ohmic contact formation. We expand on these discussions through thorough investigation of the chemical composition of the contacts via depth-resolved x-ray photoelectron spectroscopy (XPS). This allows us to identify slight variations in the Ti and Ga bonding information that indicate differences in oxidation state and chemical structure between contacts formed on surfaces that have been exposed to the liftoff process and surfaces that are as-grown or have been cleaned by Ga-flux polishing.¹⁴ Specifically, we note incomplete oxidation of the Ti layer at the interface, and the appearance of an additional higher binding energy component to the Ga peak that indicates some chemical modification of the Ga₂O₃ surface.

2. SAMPLE GROWTH AND FABRICATION

Samples A, B, and E were grown by metal-organic chemical vapor deposition (MOCVD) in an Agnitron Agilis 100 MOCVD system. Triethylgallium (TEGa) and oxygen in an argon carrier gas were used as the growth precursors, with the in-situ Si-doping provided by silane (25 ppm SiH₄ in Ar). Samples were grown on Fe-doped (010) β -Ga₂O₃ seminsulating substrates that were dipped in a 48% HF bath for 30 minutes immediately prior to loading into the reactor to reduce the interfacial silicon.²

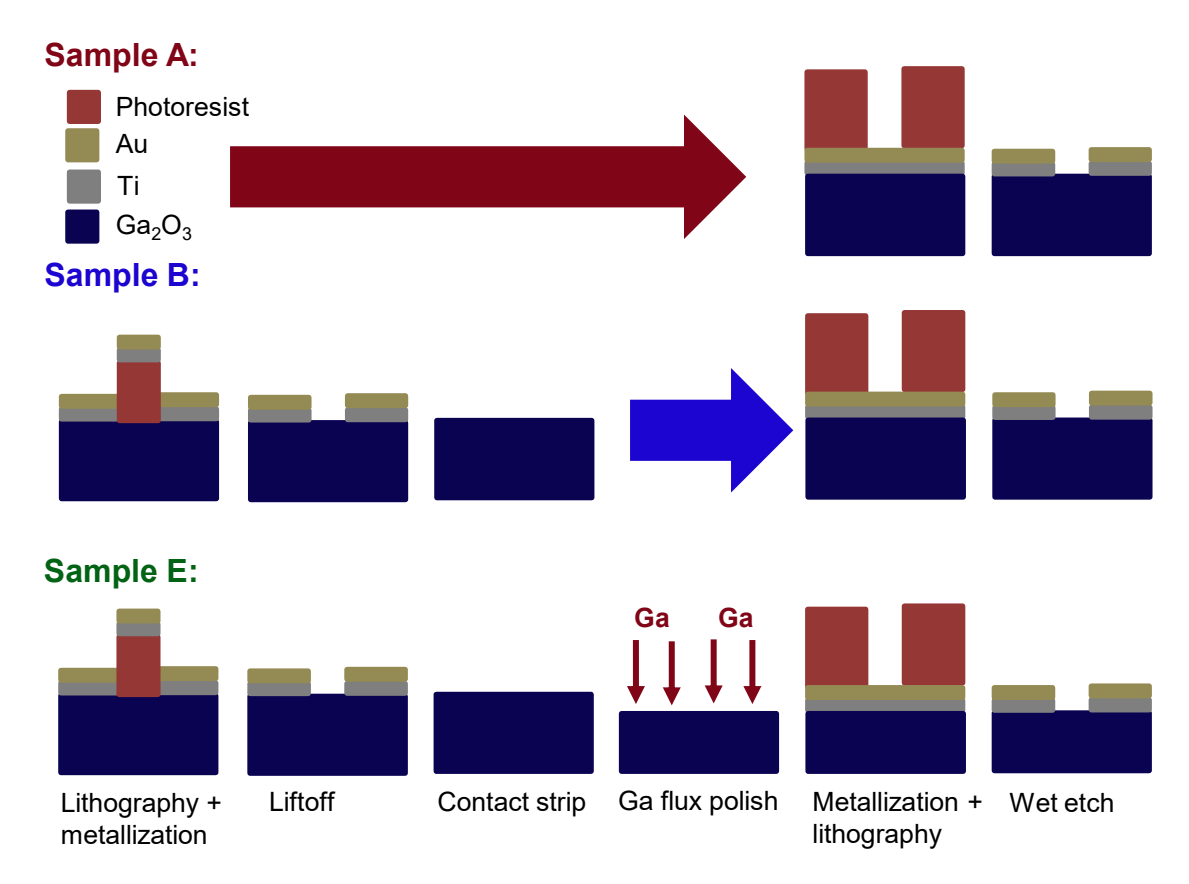


Figure 1. Diagrams of the process flow for samples a) A, b) B, and c) E.

For Sample A, a 50 nm UID layer was grown followed by a 250 nm heavily doped layer, then diced in half and solvent cleaned. Additional growth details are reported elsewhere. The 2 \times 2 μ m RMS roughness measured by atomic force microscopy (AFM) was 0.9 nm. The channel charge, mobility, and sheet resistance (R_{sh}) were 7×10^{19} cm⁻³, 89.2 cm²/V-s, and 39.9 Ω / \square from Hall measurements on an immediately prior grown 5 \times 5 mm calibration sample. Following growth, a blanket 10/110 nm Ti/Au layer was deposited by electron-beam evaporation in a load-locked Angstrom evaporator. Circular transfer length method (CTLM) patterns were defined using contact photolithography, then wet etched in 45 seconds of

TFA Gold Etchant followed by 90 seconds 30:1 buffered oxide etch (BOE) to form the contact pads. Fig. 1a shows the process flow for sample A.

For sample B, the UID layer was grown 102.5 nm thick, followed by a 160 nm heavily doped layer. The $2 \times 2 \mu m$ RMS roughness measured by AFM was 0.4 nm. The channel charge, mobility, and sheet resistance (R_{sh}) were 9.8×10^{19} cm⁻³, 79.5 cm²/V-s, and 52.3 Ω / \square from Hall measurements on an immediately prior grown 5×5 mm calibration sample. For sample E, a 102.5 nm UID layer was again grown followed by a 222.5 nm heavily doped layer. The $2 \times 2 \mu m$ RMS roughness measured by AFM was 0.7 nm. The channel charge, mobility, and sheet resistance (R_{sh}) were 5.3×10^{19} cm⁻³, 75.8 cm²/V-s, and 68.7Ω / \square from Hall measurements. Samples B and E were first mesa-isolated by ICP-RIE etching using a BCl₃/Ar chemistry with Ti/Ni hard mask to define both linear and circular TLM patterns. TLM liftoff patterns were defined by contact lithography, followed by ohmic contact metallization using electron-beam evaporation of 50/110 nm Ti/Au in a CVC SC4500 bell jar evaporator. The contact metals were then lifted off in Microposit Remover 1165. The TLM patterns were measured. Subsequently, the TLM metal pads were removed by 5 minutes of 1:1 HF:HNO3 followed by 30 seconds in TFA Au Etchant to remove re-deposited Au. The sample surfaces were further cleaned with 9 minutes of ozone followed by 5 minutes in 49% HF to further remove any residual surface contamination, eg. photoresist residue.

Sample	Doping [cm ⁻³]	Thickness [nm]	$R_{sh} [\Omega/\Box]$	Process	$R_c [\Omega\text{-mm}]$
A	7×10^{19}	250	40	Metal-first	0.26
B_L	1×10^{20}	160	50	Liftoff	-
B_{L+M}				Metal-first	-
E_L	5×10^{19}	220	76	Liftoff	-
E_{L+M}				Metal-first	0.46

Table 1. Summary of sample growth, processing, and contact resistances.

Sample B was immediately loaded into the load-locked evaporator and 10/110 nm Ti/Au was deposited and patterned into TLM patterns as for sample A. Fig. 1b shows the process flow for sample B (mesa isolation not shown). Sample E was Ga-flux polished for 4 minutes in a Veeco Gen 930 molecular beam epitaxy (MBE) system with an etch rate of approximately 2.5 nm/min. The sample was soaked in 37% HCl for 15 minutes to remove the backside indium coating, then loaded into the load-locked evaporator and 10/110 nm Ti/Au was deposited and patterned into TLM patterns as for samples A and B. Fig. 1c shows the process flow for sample E (mesa isolation not shown). The sample details for samples A, B, and E are summarized in Tab. 1.

3. CTLM CONTACT RESISTANCE MEASUREMENTS

The TLM patterns were measured in a four-point probe configuration using a Keithley 4200 source-meter with a current compliance of 100 mA. The measured CTLM patterns had an inner radius of 50 μ m and a pad spacing of 3 - 12 \pm 0.2 μ m. The contact resistance (R_c) was extracted using the correction factor as outlined by M. Krämer. ¹⁵

Fig. 2a summarizes the contact behavior measured on a 5 μ m pad spacing for samples A, B, and E both after the original contact process and after any successive contact re-processing. For samples B and E, the original contacts are non-conductive or yield very low current with highly rectifying Schottky behavior. Sample B does not improve with metal-first reprocessing; sample E, however, yields nearly-linear ohmic behavior with the addition of a Ga-flux polishing step. Sample A yields similar nearly-linear ohmic behavior which indicates (1) that the liftoff process leads to surface contamination/modification that impairs ohmic contact formation and (2) Ga-flux polishing is effective at removing the modified layer whereas conventional cleaning methods are insufficient.

For sample A, non-alloyed R_c extracted by CTLM is 0.26 Ω -mm and R_{sh} is 43 Ω/\square , which is comparable to the R_{sh} extracted by Hall as-grown (Fig. 2b). Sample E yields a higher non-alloyed R_c of 0.64 Ω -mm and R_{sh} of 85 Ω/\square , likely due to the lower doping density which creates a thicker tunneling barrier (Fig. 2c). The sheet resistance is slightly higher than, but similar to, that of the as-grown sample, perhaps due to incomplete removal of the modified layer or non-optimized etching during the Ga-flux polish. In depth contact resistance studies on these and other samples are reported elsewhere. Fig. 3 benchmarks reported contact resistance in Ω -mm of Ti/Au contacts to (010) β -Ga₂O₃ relative to the doping density directly underneath the contact. These contacts are in class with other reported low-resistance ohmic contacts.

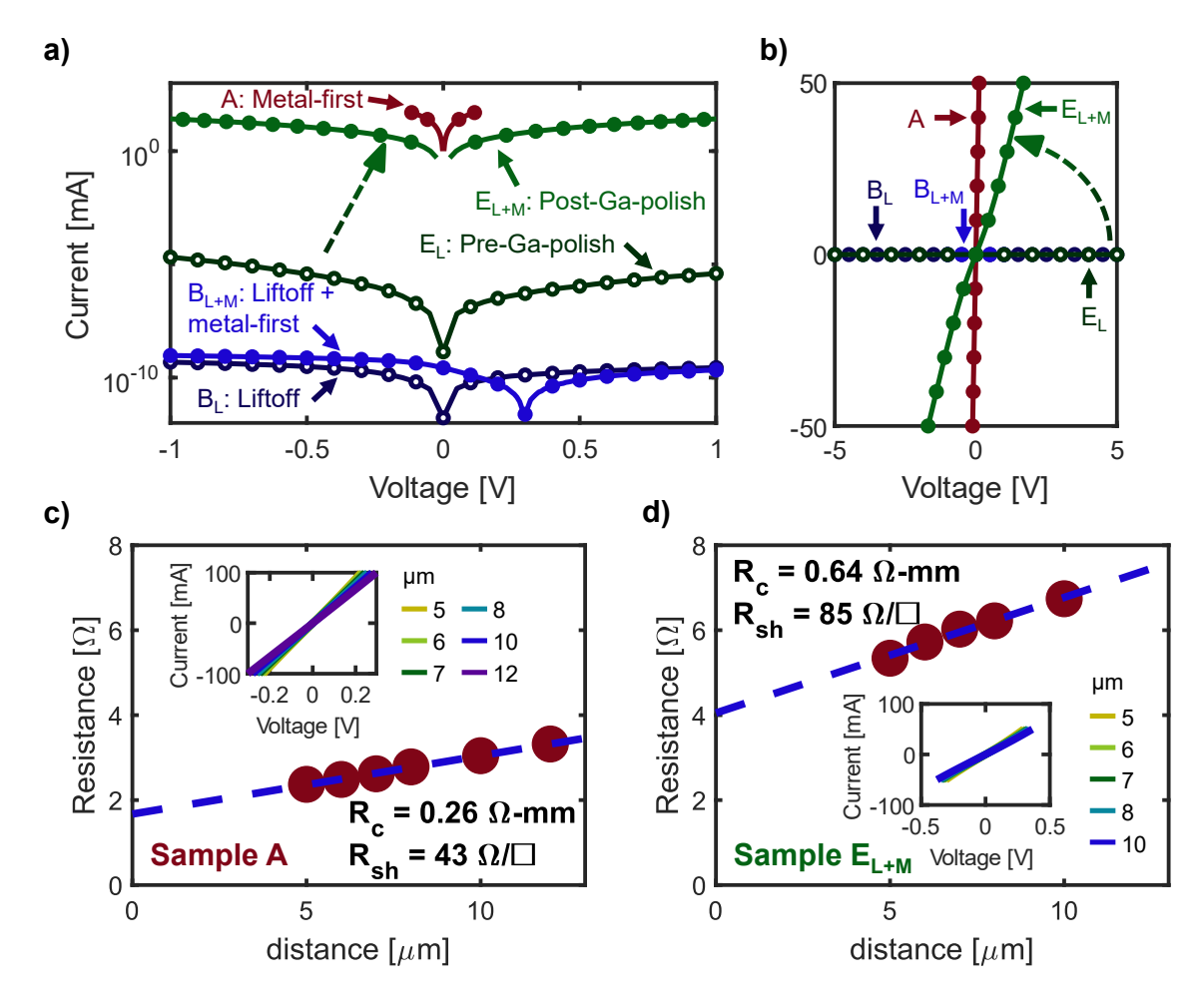


Figure 2. a) I-V curves for sample A (red), sample B (blue) after original liftoff processing (open symbols) and after metal-first reprocessing (filled symbols) and sample E (green) after original liftoff processing (open symbols) and after Ga-flux polishing and metal-first reprocessing (filled symbols). b) CTLM measurements for sample A yield an R_c of 0.26 Ω-mm, R_{sh} of 43 Ω/ \square , and ρ_c of 4.7 × 10⁻⁵. c) CTLM measurements for sample E after re-processing yield an R_c of 0.64 Ω-mm, R_{sh} of 85 Ω/ \square , and ρ_c of 1.6 × 10⁻⁵. Graphics adapted from Smith, *et al.*, Appl. Phys. Lett. **123**, 242101 (2023) with the permission of AIP Publishing.

4. XPS CHEMICAL STRUCTURE ANALYSIS

The XPS measurements were performed on a Thermo Nexsa G2 XPS with an Al-K α (1486.6 nm) source. The success of Ga-flux polishing at recovering the quality of the Ga_2O_3 surface for sample E implies that the conventional liftoff process somehow modifies the surface, creating an interfacial layer that inhibits contact performance and must be physically removed in order to allow subsequent ohmic contact formation. To this end, depth-resolved XPS was performed on samples A, B, and E to determine the chemical composition of this interfacial layer. An Ar ion gun was used to sputter the contacts between measurements of the XPS spectra. A monatomic beam was used to sputter through the majority of the Au top coating efficiently before switching to a cluster source near the beginning of the Ti layer in order to prevent damage to the sample and resulting reduction in the oxidation state of oxidized species such as Ti and Ga.

Survey spectra were taken over the full measurement range periodically in order to determine the elemental composition over the depth of the contact and specifically to identify any foreign contaminants such as carbon that might have been introduced at the metal-semiconductor interface by the liftoff process. Fig. 4 shows the depth profile of the elemental composition of sample B after metal-first reprocessing. While adventitious carbon is present on the surface from the atmosphere prior to etching, no additional carbon signatures are observed within the contact structure, nor are any other elements observed beyond the expected Au, Ti, Ga, and O. Any contaminants that may be present are therefore below the

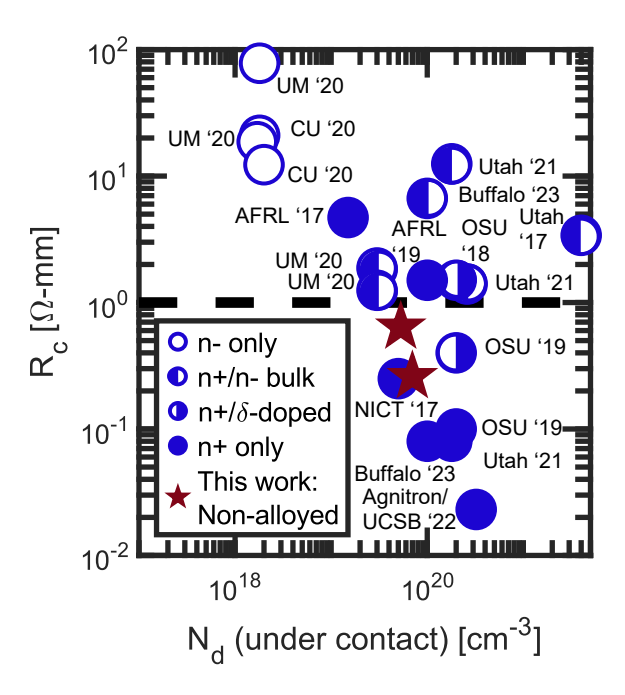


Figure 3. Benchmarking of Ti/Au ohmic contacts on (010) β -Ga₂O₃ with respect to the doping level underneath the contacts. ^{13,16–26} Graphics adapted from Smith, *et al.*, Appl. Phys. Lett. **123**, 242101 (2023) with the permission of AIP Publishing.

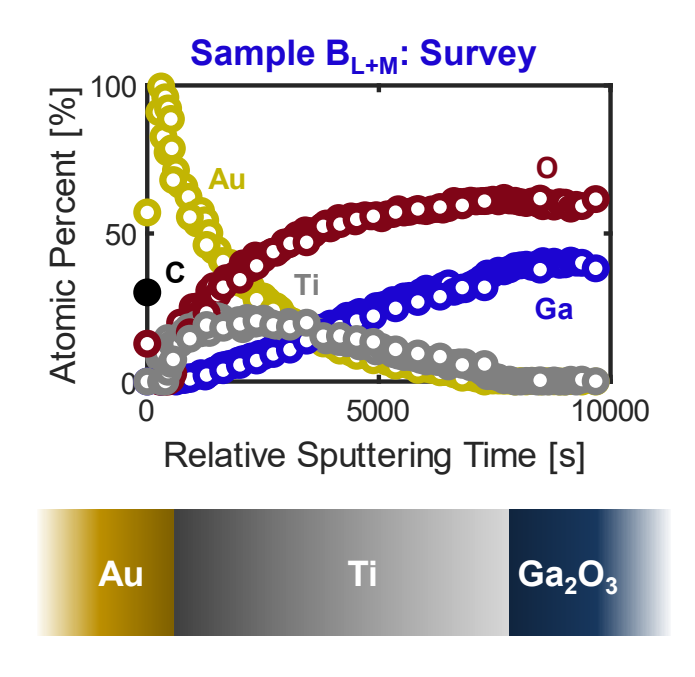


Figure 4. Depth-resolved elemental composition of sample B. Before etching (t=0), a layer of adventitious carbon from the atmosphere is present. After this layer is removed, only Au, Ti, Ga, and O are detected. No foreign contaminants are detected. Samples A and E yield comparable results. Graphics adapted from Smith, *et al.*, Appl. Phys. Lett. **123**, 242101 (2023) with the permission of AIP Publishing.

detection limit (0.1 - 1 atomic percent). The overlap between the Au, Ti, and Ga signals is due to sample charging despite the Ar ion flood gun charge compensation system, which results in a spatially non-uniform sputtering rate. Also, while XPS is surface sensitive, the photo-electron escape depth is a few nanometers (0.5 - 5 nm), material and binding energy dependent), so some overlap is expected, especially for materials with binding energies at the lower (Au) and higher (Ga) ends of the measurement range. The long Au tail can also be partially attributed to redposition of the sputtered Au, as it is

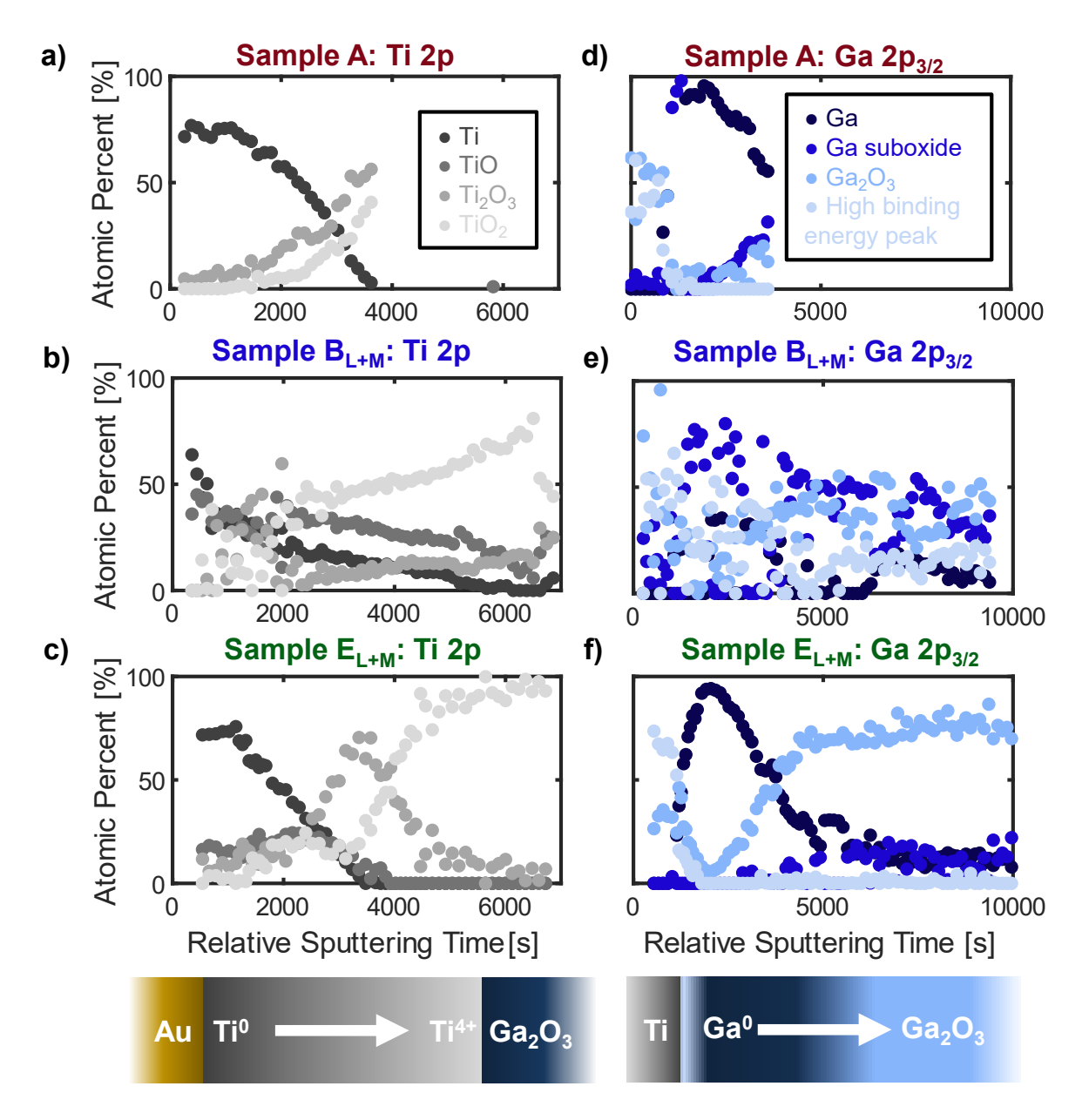


Figure 5. Chemical bonding analysis of the Ti 2p peak for sample a) A, b) B, and c) E. The oxidation state of the Ti is plotted over the entire sputtering range where the Ti peak is detected. For sample C, the Ti layer is fully oxidized to Ti^{4+} for approximately 2-3 nm near the Ga_2O_3 interface. For sample B, the Ti is partially oxidized all the way to the Ga_2O_3 interface. The data from sample A is truncated due to a shortened experimental run; however the available data is similar to sample E. Chemical bonding analysis of the Ga_2O_3 peak for sample d) A, e) B, and f) E. The oxidation state of the Ga_3O_3 is plotted over the entire sputtering range where the Ga_3O_3 is partially reduced to Ga_3O_3 and Ga_3O_3 suboxide at the Ti interface due to preferential oxidation of Ti over Ga_3O_3 . For sample B, the Ga_3O_3 oxidation profile is disordered and includes the presence of a fourth peak at higher binding energy.

a softer material. The depth profiles for samples A and E are comparable to sample B.

Analysis of the chemical bonding state of the Ti is performed by fitting the Ti 2p peak assuming four possible oxidation states: Ti^0 , Ti^{2+} , Ti^{3+} , and Ti^{4+} , and by fitting the Ti $2p_{3/2}$ and Ti $2p_{1/2}$ peaks together as described by Biesinger, *et al.*.²⁷ For sample E, the shift in binding energy indicates that the Ti oxidation state increases from mostly Ti^0 near the Au layer to entirely Ti^{4+} near the Ga_2O_3 surface (Fig. 5c). Ti is preferentially oxidized over Ga due to the lower Gibbs free energy of formation. The titanium layer (10 nm as-deposited) is at least partially oxidized and approximately 2-3 nm near the surface are fully oxidized to TiO_2 . This corroborates previous STEM results that report formation of a few nanometer $Ti - TiO_x$ layer in non-alloyed contacts to Ga_2O_3 at room temperature.²⁸ The data from sample A is truncated due to a shortened XPS run; however, the available data is comparable to that for sample E (Fig. 5a). For sample B, the titanium layer is also partially oxidized; however, the Ti 2p peak position indicates that the Ti layer is not fully oxidized to Ti^{4+} even at the Ga_2O_3 interface (Fig. 5b). Formation of low resistance ohmic contacts to Ga_2O_3 using Ti has been at least partially attributed to the formation of a TiO_2 intermediate semiconductor layer.^{29,30} The incomplete oxidation of the Ti layer in sample B may therefore form a lower quality semiconductor layer and contribute to the poor contact formation.

Analyis of the Ga bonding state is similarly performed by fitting the Ga $2p_{3/2}$ peak. Due to extensive sputtering, some sample charging is expected, which will lead to an overall upwards shift in binding energy across the spectrum. As there is no C 1s peak available, the binding energy axis is calibrated to the Ti $2p_{3/2}$ peak location. The Ga $2p_{3/2}$ peak is fitted with four possible chemical states identified by Hinkle, *et al.*: Ga^0 , Ga suboxide, Ga_2O_3 , and a higher binding energy peak that is not identified but one possibility that is raised is a Ga - OH complex. Hydrogen cannot be detected by XPS, so the presence of any H must be inferred. For sample E, the $Ga 2p_{3/2}$ peak shifts to lower binding energies near the Ti interface, indicating that, as the Ti is oxidized to TiO_2 , the Ga_2O_3 as expected is reduced to Ga^0 and Ga suboxide (Fig. 5f). No component from the unidentified high binding energy peak is observed. Sample A is again comparable to sample E (Fig. 5d). For sample B, however, the oxidation state of the Ga is a disorded combination of all four components near the Ti interface (Fig. 5e). Further into the Ga layer, the chemical composition is mostly a mixture of Ga suboxide and Ga_2O_3 , with some Ga^0 and high binding energy components. The apparent incomplete and disordered oxidation, as well as the presence of this unidentified component, may be a signature of the surface layer modification implied by the contact resistance measurements.

5. CONCLUSIONS

Metal contacts to β -Ga₂O₃ have been shown to depend heavily on device processing. The conventional liftoff process results in apparent modification to the Ga₂O₃ surface that inhibits ohmic contact formation. Conventional cleaning methods are insufficient to remove the contaminated layer; however, removal of the top 10 nanometers by Ga-flux polishing apparently recovers the quality of the Ga₂O₃ surface and allows for subsequent formation of low resistance ohmic contacts using a metal-first process. Depth-resolved XPS characterization of contacts fabricated on a surface modified by the liftoff process and a surface that has been recovered by Ga-flux polishing suggests that the liftoff process modifies the Ga₂O₃ surface in a manner that prevents complete oxidation of the titanium at the Ga₂O₃ interface and may result in the poor contacts. These results indicate that the Ga₂O₃ surface must be treated with great care and all process steps must be scrutinized in order to form high-quality metal-semiconductor interfaces suitable for contacts in high-performance RF and power devices.

6. ACKNOWLEDGEMENTS

This work was in part supported by ACCESS, an AFOSR Center of Excellence (FA9550-18-1-0529). This work was supported in part by SUPREME, one of seven centers in JUMP 2.0, a Semiconductor Research Corporation (SRC) program sponsored by DARPA. This work used facilities and instrumentation supported by NSF through the Cornell University Materials Research Science and Engineering Center DMR-1719875. The device fabrication was performed in part at the Cornell Nanoscale Facility, a NNCI member supported by NSF grant NNCI-2025233.

REFERENCES

[1] Gann, K. R., Pieczulewski, N., Gorsak, C. A., Heinselman, K., Asel, T. J., Noesges, B. A., Smith, K. T., Dryden, D. M., Xing, H. G., Nair, H. P., Muller, D. A., and Thompson, M. O., "Silicon implantation and annealing in β -Ga₂O₃: Role of ambient, temperature, and time," *J. Appl. Phys.* **135**, 015302 (2024).

- [2] Bhattacharyya, A., Peterson, C., Itoh, T., Roy, S., Cooke, J., Rebolloa, S., Ranga, P., Sensale-Rodriguez, B., and Krishnamoorthy, S., "Enhancing the electron mobility in Si-doped (010) β-Ga₂O₃ films with low-temperature buffer layers," APL Mater. 11, 021110 (2023).
- [3] Li, W., Nomoto, K., Nakamura, T., Jena, D., and Xing, H. G., "Single and multi-fin normally-off Ga₂O₃ vertical transistors with a breakdown voltage over 2.6 kv," *IEEE Int. Electron Devices Meeting (IEDM)*, 12.1.4–12.4.4 (2019).
- [4] Green, A. J., Chabak, K. D., Heller, E. R., Fitch, R. C., Baldini, M., Fiedler, A., Irmscher, K., Wagner, G., Galazka, Z., Tetlak, S. E., Crespo, A., Leedy, K., and Jessen, G. H., "3.8-mv/cm breakdown strength of MOVPE-grown Sn-doped β-Ga₂O₃ MOSFETs," *IEEE Electron Device Lett.* 37, 902 (2016).
- [5] Lyle, L. A. M., "Critical review of ohmic and schottky contacts to β -Ga₂O₃," *J. Vac. Sci. Technol. A* **40**, 060802 (2022).
- [6] Farzana, E., Zhang, Z., Paul, P. K., Arehart, A. R., and Ringel, S. A., "Influence of metal choice on (010) β-Ga₂O₃ Schottky diode properties," *Appl. Phys. Lett.* **40**, 060802 (2017).
- [7] Yao, Y., Gangireddy, R., Kim, J., Das, K. K., Davis, R. F., and Porter, L. M., "Electrical behavior of β-Ga₂O₃ schottky diodes with different Schottky metals," *J. Vac. Sci. Technol. B* **35**, 03D113 (2017).
- [8] Polyakov, A. Y., Smirnov, N. B., Shchemerov, I. V., Pearton, S. J., Ren, F., Chernykh, A. V., and Kochkova, A. I., "Electrical properties of bulk semi-insulating β-Ga₂O₃ (Fe)," *Appl. Phys. Lett.* **113**, 142102 (2018).
- [9] Polyakov, A. Y., Lee, I.-H., Smirnov, N. B., Yakimov, E. B., Shchemerov, I. V., Chernykh, A. V., Kochkova, A. I., Vasilev, A. A., Ren, F., P. H. Carey, I., and Pearton, S. J., "Hydrogen plasma treatment of β-Ga₂O₃: Changes in electrical properties and deep trap spectra," *Appl. Phys. Lett.* **115**, 032101 (2019).
- [10] Taka, B. R., Dewanb, S., Goyalc, A., Pathaka, R., Guptab, V., Kapoorc, A. K., Nagarajand, S., and Singh, R., "Point defects induced work function modulation of β-Ga₂O₃," *Appl. Surf. Sci.* **465**, 973 978 (2019).
- [11] Li, W., Saraswat, D., Long, Y., Nomoto, K., Jena, D., and Xing, H. G., "Near-ideal reverse leakage current and practical maximum electric field in β -Ga₂O₃ Schottky barrier diodes," *Appl. Phys. Lett.* **116**, 192101 (2020).
- [12] Smith, K. T., Gorsak, C. A., Kalra, A., Cromer, B., Azizie, K., Dryden, D. M., Schlom, D., Jena, D., Nair, H. P., and Xing, H. G., "Non-alloyed ohmic contacts to (010) β -Ga₂O₃ with low contact resistance," *Appl. Phys. Lett.* **123**, 242101 (2023).
- [13] Alema, F., Peterson, C., Bhattacharyya, A., Roy, S., Krishnamoorthy, S., and Osinsky, A., "Low resistance ohmic contact on epitaxial MOVPE grown β -Ga₂O₃ and β -(Al_xGa_{1-x})₂O₃ films," *IEEE Electron Device Lett.* **43**, 1649 (2022).
- [14] Kalra, A., Gallium beam etching of gallium oxide in a molecular beam epitaxy system, m.S. thesis, Cornell University (2023).
- [15] Krämer, M. C. J. C. M., Fabrication and characterization of metal-semiconductor contacts for application in $Al_xGa_{1-x}N/GaN$ HEMTs, m.S. thesis, Technical University of Eindhoven (2000).
- [16] Chabak, K., Green, A., Moser, N., Tetlak, S., McCandless, J., Leedy, K., Fitch, R., Crespo, A., and Jessen, G., "Gate-recessed, laterally-scaled β -Ga₂O₃ MOSFETs with high-voltage enhancement-mode operation," *IEEE Device. Res. Conf. (DRC)*, 1–2 (2017).
- [17] Wong, M. H., Nakata, Y., Kuramata, A., Yamakoshi, S., and Higashiwaki, M., "Enhancement-mode Ga₂O₃ MOS-FETs with Si-ion- implanted source and drain," *Appl. Phys. Express* **10**, 041101 (2017).
- [18] Zeng, K., Wallace, J. S., Heimburger, C., Sasaki, K., Kuramata, A., Masui, T., Gardella, J. A., and Singisetti, U., "Ga₂O₃ MOSFETs using spin-on-glass source/drain doping technology," *IEEE Electron Device Lett.* **38**, 513 (2017).
- [19] Xia, Z., Joishi, C., Krishnamoorthy, S., Bajaj, S., Zhang, Y., Brenner, M., Lodha, S., and Rajan, S., "Delta doped β-Ga₂O₃ field effect transistors with regrown ohmic contacts," *IEEE Electron Device Lett.* **39**, 568 (2018).
- [20] Liddy, K. J., Green, A. J., Hendricks, N. S., Heller, E. R., Moser, N. A., Leedy, K. D., Popp, A., Lindquist, M. T., Tetlak, S. E., Wagner, G., Chabak, K. D., and Jessen, G. H., "Thin channel β-Ga₂O₃ MOSFETs with self-aligned refractory metal gates," *Appl. Phys. Express* **12**, 126501 (2019).
- [21] Xia, Z., Xue, H., Joishi, C., McGlone, J., Kalarickal, N. K., Sohei, S. H., Brenner, M., Arehart, A., Ringel, S., Lodha, S., Lu, W., and Rajan, S., "β-Ga₂O₃ delta-doped field-effect transistors with current gain cutoff frequency of 27 GHz," *IEEE Electron Device Lett.* **40**, 1052 (2019).
- [22] Smith, K., Long, E., Li, W., Nomoto, K., Jena, D., and Xing, H. G., "Threshold voltage modulation by fin width design in lateral β -Ga₂O₃ transistors on (010) Ga₂O₃ substrates," *Semiconductor Interface Specialists Conference* (SISC) (2020).

- [23] Bhattacharyya, A., Roy, S., Ranga, P., Shoemaker, D., Song, Y., Lundh, J. S., Choi, S., and Krishnamoorthy, S., "130 ma mm⁻¹ β -Ga₂O₃ metal semiconductor field effect transistor with low-temperature metalorganic vapor phase epitaxy-regrown ohmic contacts," *Appl. Phys. Express* **14**, 076502 (2021).
- [24] Bhattacharyya, A., Ranga, P., Roy, S., Peterson, C., Alema, F., Seryogin, G., Osinsky, A., and Krishnamoorthy, S., "Multi-kV class β -Ga₂O₃ MESFETs with a lateral figure of merit up to 355 MW/cm²," *IEEE Electron Device Lett.* **42**, 1272 (2021).
- [25] Long, E., Beta-gallium oxide lateral field-effect transistors: fabrication and performance, m.S. thesis, Cornell University (2021).
- [26] Saha, C. N., Vaidya, A., Bhuiyan, A. F. M. A. U., Meng, L., Sharma, S., Zhao, H., and Singisetti, U., "Scaled β-Ga₂O₃ thin channel MOSFET with 5.4 MV/cm average breakdown field and near 50 GHz f_{MAX}," *Appl. Phys. Lett.* **122**, 182106 (2023).
- [27] Biesinger, M. C., Lau, L. W. M., Gerson, A. R., and Smart, R. S. C., "Resolving surface chemical states in XPS analysis of first row transition metals, oxides and hydroxides: Sc, Ti, V, Cu and Zn," *Appl. Surf. Sci.* **257**, 887 898 (2010).
- [28] Lee, M. H. and Peterson, R. L., "Annealing induced interfacial evolution of titanium/gold metallization on unintentionally doped β-Ga₂O₃," *J. Solid State Sci. Technol.* **8**, Q3176 (2019).
- [29] Lee, M. H. and Peterson, R. L., "Interfacial reactions of titanium/gold ohmic contacts with Sn-doped β -Ga₂O₃," *APL Mater.* 7, 022524 (2019).
- [30] Lee, M. H. and Peterson, R. L., "Process and characterization of ohmic contacts for beta-phase gallium oxide," *J. Mater. Res.* **36**, 4771 (2021).
- [31] Hinkle, C. L., Milojevic, M., Brennan, B., Sonnet, A. M., Aguirre-Tostado, F. S., Hughes, G. J., Vogel, E. M., and Wallace, R. M., "Detection of Ga suboxides and their impact on III-V passivation and Fermi-level pinning," *Appl. Phys. Lett.* **94**, 162101 (2009).